nature communications

Article

https://doi.org/10.1038/s41467-025-57764-z

FAN1-mediated translesion synthesis and POLQ/HELQ-mediated end joining generate interstrand crosslink-induced mutations

Received: 25 January 2024

Accepted: 4 March 2025

Published online: 13 March 2025

Check for updates

Jip Verschuren[1,4], Robin van Schendel[1,4], Ivo van Bostelen[1], Alex E. E. Verkennis[2], Puck Knipscheer[1,2] & Marcel Tijsterman[1,3]

To counteract the damaging effects of DNA interstrand crosslinks (ICLs), cells have evolved various specialized ICL repair pathways. However, how ICL repair impacts genetic integrity remains incompletely understood. Here, we determined the mutagenic consequences of psoralen ICL repair in the animal model *C. elegans* and identify two mutagenic repair mechanisms: (i) translesion synthesis through POLH and REV1/3-mediated bypass, leading to single nucleotide polymorphisms (SNVs), and (ii) end joining via POLQ or HELQ action resulting in deletions. While we found no role for the Fanconi anemia genes FANCD2 and FANCI, disruption of TRAIP, which triggers unloading of the CMG helicase at sites of blocked replication, led to a strikingly altered repair profile, suggesting a role for DNA replication in the etiology of ICL-induced deletions. TRAIP deficiency did not affect SNV formation; instead, we found these SNVs to depend on the functionality of the Fanconi anemia-associated nuclease FAN1.

DNA crosslinking occurs when chemical entities covalently bridge the two strands of the DNA double helix, effectively linking them together. This interstrand connection hinders the essential cellular processes of transcription and DNA replication, thereby compromising cell vitality, as well as the faithful transmission of genetic information during cell division. Sources of DNA interstrand crosslinks (ICLs) are widespread and diverse, ranging from endogenous metabolic byproducts like aldehydes to exogenous genotoxic agents such as certain chemotherapeutic drugs and environmental mutagens. Consequently, cells have evolved intricate repair mechanisms to address the challenge posed by ICLs and maintain genomic stability[1]. Failure to effectively process ICLs has detrimental consequences for human development and leads to clinical phenotypes, most notably Fanconi anemia, a genetic disorder marked by congenital abnormalities, bone marrow failure, an increased predisposition to cancer, and heightened sensitivity to crosslinking agents[2].

The pathway affected in Fanconi anemia (FA) is the most versatile and extensively studied ICL repair pathway. This FA pathway is coupled to DNA replication and activated when the replication fork encounters an ICL[3]. Convergence of dual forks at the ICL leads to the removal of the stalled replicative CMG helicase through ubiquitination by the ubiquitin ligase TRAIP and subsequent unloading by the p97 ATPase[4]. This allows further approach of the polymerase to the ICL leading to dual incisions on one of the two DNA strands, effectively unhooking the crosslink[1]. While several endonucleases have been suggested to act in this unhooking step, direct evidence only exists for the involvement of the ERCC1/XPF complex[5]. ICL unhooking results in the creation of a DNA double-strand break (DSB) in one chromatid, while the other chromatid contains the unhooked lesion[5,6]. Bypass of the adducted strand by translesion DNA synthesis[7] generates an intact duplex, which then serves as a template for the resolution of the DSB through RAD51-mediated homologous recombination (HR)[1].

The nuclease FAN1 (FANCD2 Associated Nuclease 1) has also been implicated in ICL repair. Similarly to FA proteins, FAN1 deficiency leads to chromosomal instability and mild sensitivity to a wide range of ICL-inducing agents[8–12]. However, patients with germline mutations in

[1]Department of Human Genetics, Leiden University Medical Center, Leiden, The Netherlands. [2]Oncode Institute, Hubrecht Institute–KNAW and University Medical Center Utrecht, Utrecht, The Netherlands. [3]Institute of Biology Leiden, Leiden University, Leiden, The Netherlands. [4]These authors contributed equally: Jip Verschuren, Robin van Schendel. e-mail: m.tijsterman@lumc.nl

FAN1 develop karyomegalic interstitial nephritis (KIN), a disease distinctly different from FA[8,10], suggesting that FAN1 does not act in the FA pathway. In vitro research revealed that FAN1 has a high affinity for DNA replication-mimicking branched DNA structures and can process molecules that reflect single arrested DNA replication forks using endonuclease activity[13,14], providing hints for how FAN1 may act to unhook replication-impeding ICLs.

In addition to the FA pathway, ICLs induced by psoralen/UV treatment can also be resolved by a glycosylase-mediated pathway as shown using the Xenopus egg extract system[15]. This process involves the unhooking of the ICL by Neil3-mediated cleavage of the N-glycosyl bond of one of the crosslinked thymines which does not involve DSB formation. Furthermore, in cells, it has been shown that upon encounter of a psoralen-induced ICL, part of the replisome can traverse the intact lesion. This involves replisome remodeling and the action of factors such as FANCM, FANCD2 and ATR[16,17]. In addition to replication-associated responses, also replication-independent ICL repair mechanisms have been described[1,18] but less-well studied, which are likely essential to prevent the detrimental consequences of RNA polymerase arrested at the site of the blocking lesion.

Despite tremendous progress in the understanding of the molecular steps, especially in replication-associated ICL repair, it is currently still poorly understood in what way these repair pathways contribute to the mutagenesis that is observed when cells are exposed to ICL-inducing agents. Resolution of repair intermediates through the FA pathway, for example, mainly results in either a wild-type-restoring sequence or single nucleotide variant. However, ICL-inducing agents also give rise to other types of genomic alterations such as deletions[19–22]. The mutagenic consequences of ICL-inducing agents are particularly relevant for cancer therapy, where cytostatic agents such as cisplatin can be curative. Such chemicals are proficient in killing cancer cells, but are also a major source of mutagenesis in healthy or precancerous cells, thus driving carcinogenesis[23,24]. However, it remains poorly understood to what extent this carcinogenesis is caused by ICLs, as ICL-inducing chemicals also cause other genotoxic lesions such as DNA monoadducts, intra-strand crosslinks as well as DNA-protein crosslinks.

While experiments involving the exposure of cells to ICL-inducing compounds have been very valuable in identifying ICL repair pathways, biochemical assays using unique lesions at well-defined sequence contexts have added tremendous detail to our mechanistic understanding of these pathways[25–27]. Using similar defined lesions in an in vivo setting could reveal which of these pathways are used and how this repair generates mutations. To this end, we created a novel in vivo assay using *C. elegans*: an in vitro well-studied plasmid is used to determine the products of repair of a single psoralen ICL adduct in a defined sequence context. We subsequently used this methodology to assay a variety of single and double mutant animals. We provide evidence for the involvement of POLH, POLZ, as well as for FAN1 in TLS mutagenesis, and POLQ and HELQ in deletion mutagenesis.

Results

Analysis of ICL repair at nucleotide resolution in *C. elegans*

To investigate the mutagenic consequences of ICL repair, we have developed a novel assay (Fig. 1A). Our approach involves injecting a plasmid that contains a single psoralen ICL at a defined location (called pICLpso[15]) into the gonad of *C. elegans*, along with a plasmid encoding a dominant marker gene. Plasmids injected in the gonadal syncitium concatemerize in the cytoplasm of the fertilized zygote upon nuclear envelope breakdown of the first zygotic division to form extra-chromosomal arrays[28] of, on average, 100–200 plasmid molecules[29]. These extra-chromosomal arrays remain inert in the cytoplasm but, at later stages, can behave as chromosomes that are replicated and segregated during cell division. Three days after injection, we collect those progeny of the injected animals that exhibit a rolling movement phenotype, resulting from the co-injected marker gene. Considering the concentration of injected plasmids and their relative ratio, we anticipated that each array will contain approximately 10–20 pICLpso plasmids. To determine repair outcomes, PCR is used on DNA isolated from pools of animals (typically 50–100) to amplify the region originally containing the ICL, followed by next-generation sequencing (NGS). The NGS data is subsequently bio-informatically processed using SIQ[30], which establishes mutational profiles by multi-parameter annotation of sequence reads. For purpose of clarity, the profiles are graphically represented in Tornado plots (Fig. 1B) in which the following classes of mutations are distinguished: wild-type (i.e., identical to the reference sequence), SNV (single nucleotide variant), deletions, DELINS (deletions with an insertion), and TINS (deletions with a templated insertion). Noteworthy, DELINS and TINS are not necessarily the products of different biochemistry as the difference between the two classes is that TINS have insertions that are sufficiently large to allow tracing their origin to sequences flanking the deletion junction, indicative of those sequences having served as a template in a repair reaction. The origin of the insertions in the DELINS category cannot be reliably identified primarily because they are (too) small.

Remarkably, although we injected identical plasmid molecules having a single type of ICL in a fixed sequence context, a complex spectrum of mutational outcomes was obtained. Replicate experiments produced highly similar distributions, confirming the assay to be robust and suitable to reliably capture the plethora of mutagenic repair products (Fig. 1B). Based on the fraction of specific rare outcomes we estimate that a pool of progeny indeed contains hundreds of repair products. To substantiate this interpretation, we also determined the repair spectra for progeny of individual transgenic lines (Supplemental Fig. 1), which indicated 5–15 repaired plasmids per array, and together produce an outcome spectrum similar to pooled samples.

We found deletions to represent ~60% of the mutational spectrum, comprising of 50% simple deletions, 8% DELINS and 2% TINS (Fig. 1C). Deletions of 10 bp or smaller make up for over 60% of the total amount of deletions, which are further characterized by an overrepresentation of so-called sequence microhomology at their junctions: short stretches of identical sequence that are found at either side of the ICL. Furthermore, the mutation spectrum consists of 40% non-deletion outcomes, subdivided into 20% SNVs and 20% WT outcomes. Figure 1D shows the most prevalent outcomes for each category, including the fraction of each specific outcome within the spectra. We conclude from these results that plasmid injections followed by NGS analysis of transgenic animals creates an opportunity to investigate the (potentially mutagenic) consequence of ICL repair in vivo and at nucleotide resolution.

Translesion synthesis polymerases POLH-1 and POLZ-1 bypass psoralen ICLs

The spectrum of ICL repair contains two categorically distinct classes, i.e., molecules that lost DNA (deletion, DELINS and TINS) and those that have not (wild type and SNV). These separate classes point to different repair activities as well as different repair substrates: likely a DSB and a TLS substrate. The currently prevalent model of replication-coupled ICL repair by the FA pathway describes the uncoupling of the crosslinked strands into two categorically different repair intermediates (Fig. 2A): upon replication forks converging on a replication-impeding ICL, dual incision of one strand in close proximity to the ICL generates a DSB, as well as an intact opposite DNA strand that contains the unhooked adduct[1]. These intermediates need different repair activities, but in an interdependent fashion: to allow the DSB to be repaired through homologous recombination, a donor first needs to be generated through translesion synthesis (TLS) activity across the adducted strand. *C. elegans* encodes multiple evolutionarily conserved TLS polymerases. Three Y-family polymerases have been described,

https://doi.org/10.1038/s41467-025-57764-z

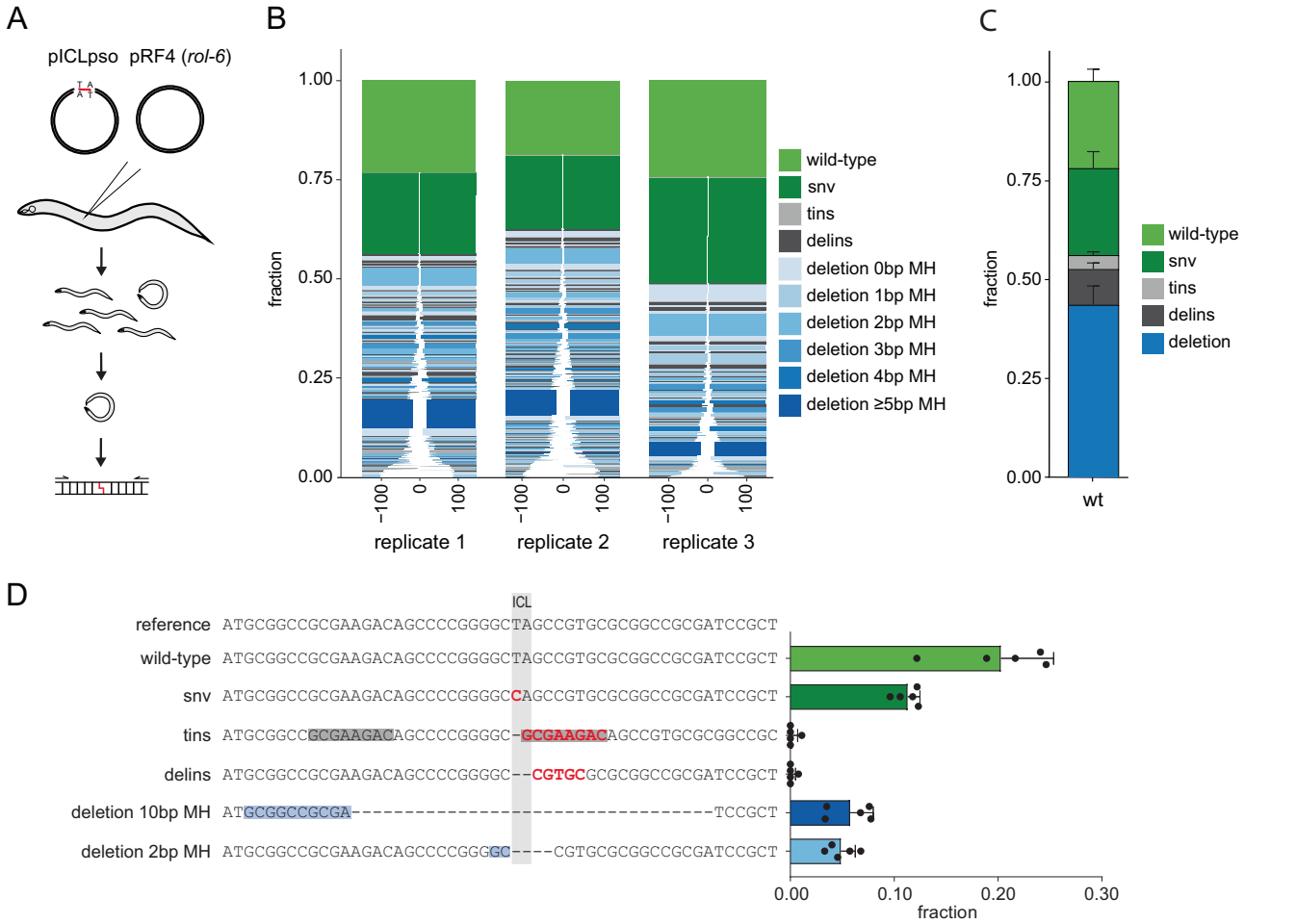

Fig. 1 | Repair outcomes of psoralen ICLs. A Schematic representation of the assay: the transgenic progeny of animals injected with plasmids are pooled. DNA is isolated and subject to analysis by NGS. **B** Tornado plots of psoralen ICL repair spectra. The outcomes of 3 replicate rounds of injections are shown, each containing 50–100 transgenic F1 animals. Sequence reads are piled, and sorted from top to bottom with respect to the distance of the sequence alteration relative to the ICL set at 0. Wild-type (WT) sequence restoring repair outcomes are depicted in light green, single nucleotide variants (SNV) in dark green. Deletion events are color-coded according to the following mutational classification: blue for simple deletions, wherein the saturation level of the blue color increases with an increasing amount of microhomology found at the deletion junction; gray for deletions that also contain an insertion (delins). The cases for which the insertion can be reliably mapped to the sequence flanking the ICL are in light gray (tins). **C** A bar graph clustering the mutation classes; same color coding as in 1B. Data are presented as mean values ± SD ($n = 3$). Each n represents the outcomes of an independent round of injections containing 50–100 transgenic F1 animals. **D** Most prevalent outcome of each mutation class. Red nucleotides indicate insertions (in SNV, delins, and tins). The template for the tins case is marked in gray, whereas sequence microhomology in deletions is marked blue. Bar graph shows the fraction of each outcome within the spectrum. Data are presented as mean values ± SD ($n = 5$). Each n represents the outcomes of an independent round of injections containing 50–100 transgenic F1 animals. Source data are provided as a Source Data file.

i.e., POLH-1, POLK-1, and REV-1[31,32] enzymes which have similar motifs for binding substrate and primer terminus, but vary with respect to nucleotide (mis)incorporation specificity[33,34]. In addition, the worm also encodes the B-family polymerase POLZ comprised of catalytic subunit REV-3[32]. Both TLS polymerase families have been found to be involved in ICL repair, both in vitro and in cells[25,35,36], making these enzymes logical candidates to underlie the restored wild-type and SNVs reaction products, making up for ~40% of repair outcomes.

To test this prediction, we generated ICL repair mutation spectra for previously described *C. elegans* TLS mutants[31,32]. The ICL repair spectrum obtained from POLK-1 deficient animals (*polk-1*) was marginally different from wild-type animals (Fig. 2B). In contrast, loss of POLH-1 dramatically changed the repair profile: wild-type and SNV outcomes were greatly reduced in *polh-1* mutant animals (Fig. 2B, C), arguing that POLH-1 is the TLS polymerase responsible for bypass of a lesion that is generated at psoralen ICLs. The observation that the repair outcomes that are reduced in *polh-1* either have a SNV at the ICL position or reflect the original sequence may argue that POLH-1 has a 50% error rate in bypassing ICL repair intermediates. Alternatively, individual psoralen ICLs may be converted either in a mutagenic or in a non-mutagenic TLS substrate.

We next determined the ICL repair spectrum in *rev-3* mutant animals, which lack the enzymatic activity of POLZ, and found it to resemble that of *polh-1* mutants: an almost complete absence of SNV and wild-type outcomes. In support of the notion that POLZ is critical for the bypass of psoralen ICL intermediates, also a complete loss of both wild-type and SNV outcomes was found in animals mutated for *rev-1*, the Y-family polymerase that is (non-catalytically) required for POLZ functionality[37]. Evaluating the types of SNVs, we further conclude that the concerted action of POLH-1 and POLZ predominantly leads to incorporation of an adenosine or a guanine across the originally crosslinked thymines (Fig. 2D). While POLZ deficient animals are completely devoid of mutagenic TLS, POLH-1 deficient animals still have some residual ability in bypass. Given that REV-1 has only cytidyl transferase activity, the logical candidate for the residual activity is POLK, a notion we have not further explored.

https://doi.org/10.1038/s41467-025-57764-z

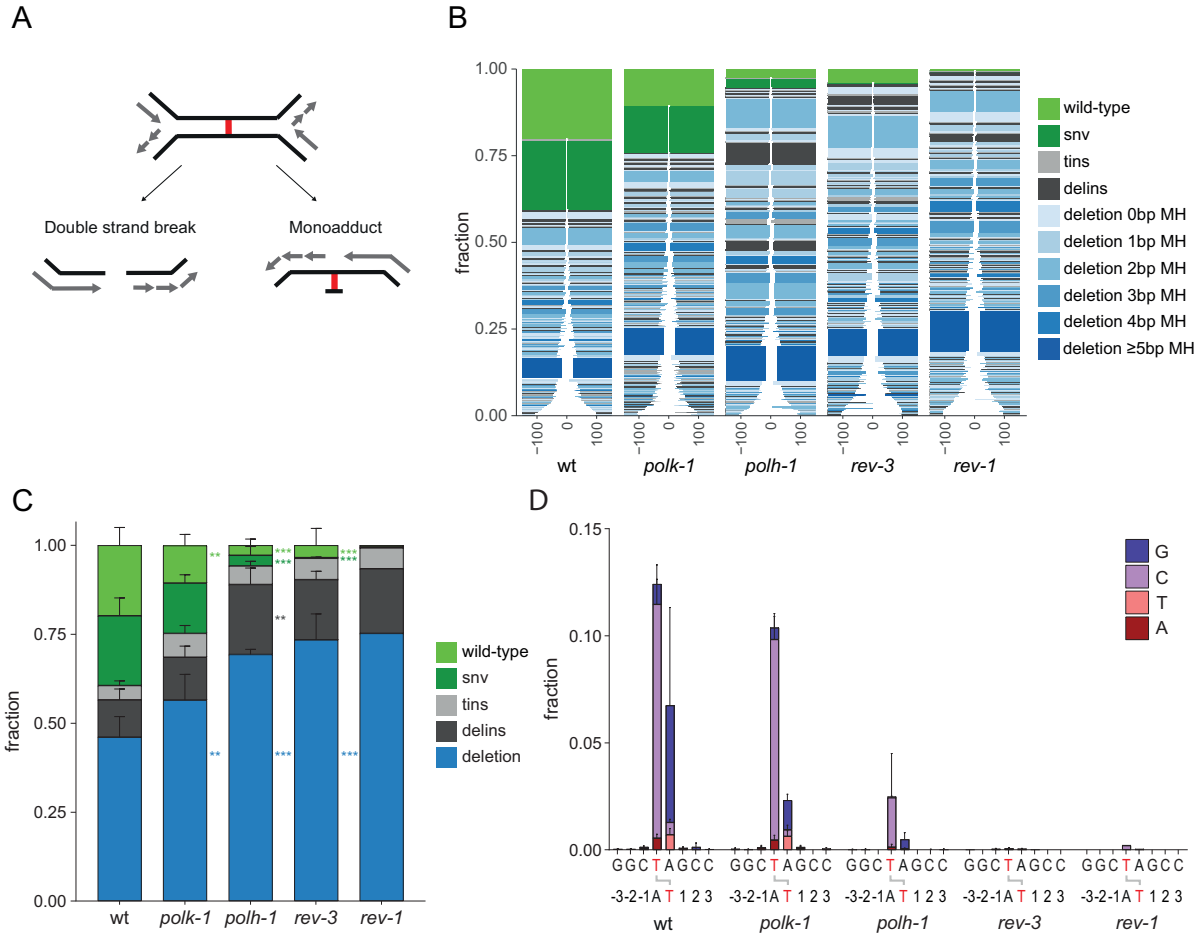

Fig. 2 | Translesion synthesis across psoralen ICLs. A Schematic model for how converging replication forks may lead to two distinct repair substrates upon incision on either side of the ICL. **B** Tornado plots and **C** bar graphs representing the mutational spectrum for wild-type ($n = 5$), *polk-1* ($n = 3$), *polh-1* ($n = 3$), *rev-3* ($n = 3$) and *rev-1* ($n = 2$) mutant animals. WT N2 vs. *polk-1*: $p = 0.012$, delins N2 vs. *polh-1*: $p = 0.0177$, deletion N2 vs *polk-1*: $p = 0.0199$ (*$P < 0.05$, ***$P < 0.001$; Two-Way ANOVA test, Dunnett's multiple comparisons test). Data are presented as mean values ± SD (for $n > 2$). **D** Histogram representing the SNV distribution at the indicated position for the indicated genotypes (wild-type ($n = 5$), *polk-1* ($n = 3$), *polh-1* ($n = 3$), *rev-3* ($n = 3$) and *rev-1* ($n = 2$)). Crosslinked thymines within the psoralen ICL are in red. Y-axis represents the fraction of the total mutation spectrum. Data are presented as mean values ± SD (for $n > 2$). Source data are provided as a Source Data file.

ICL-induced DNA breaks are repaired by TMEJ and MMEJ

Having identified the proteins that produce SNVs and wild-type-restoring repair products, we next wished to investigate the genetic requirements for the other outcomes, i.e., deletions with or without having additional insertions. Deletions are typically the product of end joining of DNA breaks, and given that the deletions produced at psoralen ICLs are characterized by an overrepresentation of microhomology (Fig. 1B; only 20% of deletions are completely devoid of MH at the junctions), and the occasional presence of (templated) insertions, polymerase theta-mediated end joining (TMEJ) is a logical candidate; both these features are hallmarks of TMEJ action[19,38,39]. To test this prediction, we established the outcome profile for psoralen ICL repair in *polq-1* mutant animals and found an almost complete absence of deletions that have 1–4 bp of MH at the junction (Fig. 3A–C). Also deletions with (templated) insertions are absent in the spectrum. We thus conclude that the vast majority of deletion products are the action of TMEJ. However, two specific deletions appear to be the result of pol theta-independent repair. Both products are characterized by 10 bp of MH and thus likely results from annealing of a 10 bp direct repeat sequence present up- and downstream of the ICL (Fig. 3D). Earlier work from our lab identified the helicase HELQ-1 to be involved in end joining of DNA breaks that had such extended stretches of direct repeats in their flanking regions[40]. Indeed, we found both repair outcomes to be absent in spectra obtained from *helq-1* mutant animals, while deletions having 0 to 4 bp of MH were generated independent of HELQ-1 (Fig. 3C). We next established that the combination of TMEJ and HELQ-1-mediated end joining accounts for all deletion mutagenesis induced by psoralen ICLs, as only wild-type and SNV outcomes are found in animals mutant for both *polq-1* and *helq-1* (Fig. 3A–C). Together, our findings establish that psoralen ICLs induce two types of mutations: (i) SNVs through POLH-1- and POLZ-1-mediated TLS, and deletions (plus or minus insertions) through POLQ-1- and HELQ-1-mediated end joining.

Psoralen-induced mutagenesis is independent of Fanconi Anemia proteins

We were surprised to find such a prominent role for TMEJ in repair of psoralen ICLs, as previous work in *Xenopus leavis* egg extracts suggested a combination of TLS and error-free HR. Those activities critically relied on components of the Fanconi Anemia (FA) pathway[26]: mono-ubiquitination of FANCD2 and FANCI through the FA core complex creates a scaffold for the endonuclease complex SLX4/XPF-ERCC1, to initiate ICL unhooking and subsequent repair[5,41]. To test the involvement of the Fanconi anemia pathway in the repair of psoralen ICLs, we assayed animals that are genetically deficient for FANCD2 or FANCI, i.e., *fcd-2* and *fnci-1* mutant animals, respectively[42]. We

https://doi.org/10.1038/s41467-025-57764-z

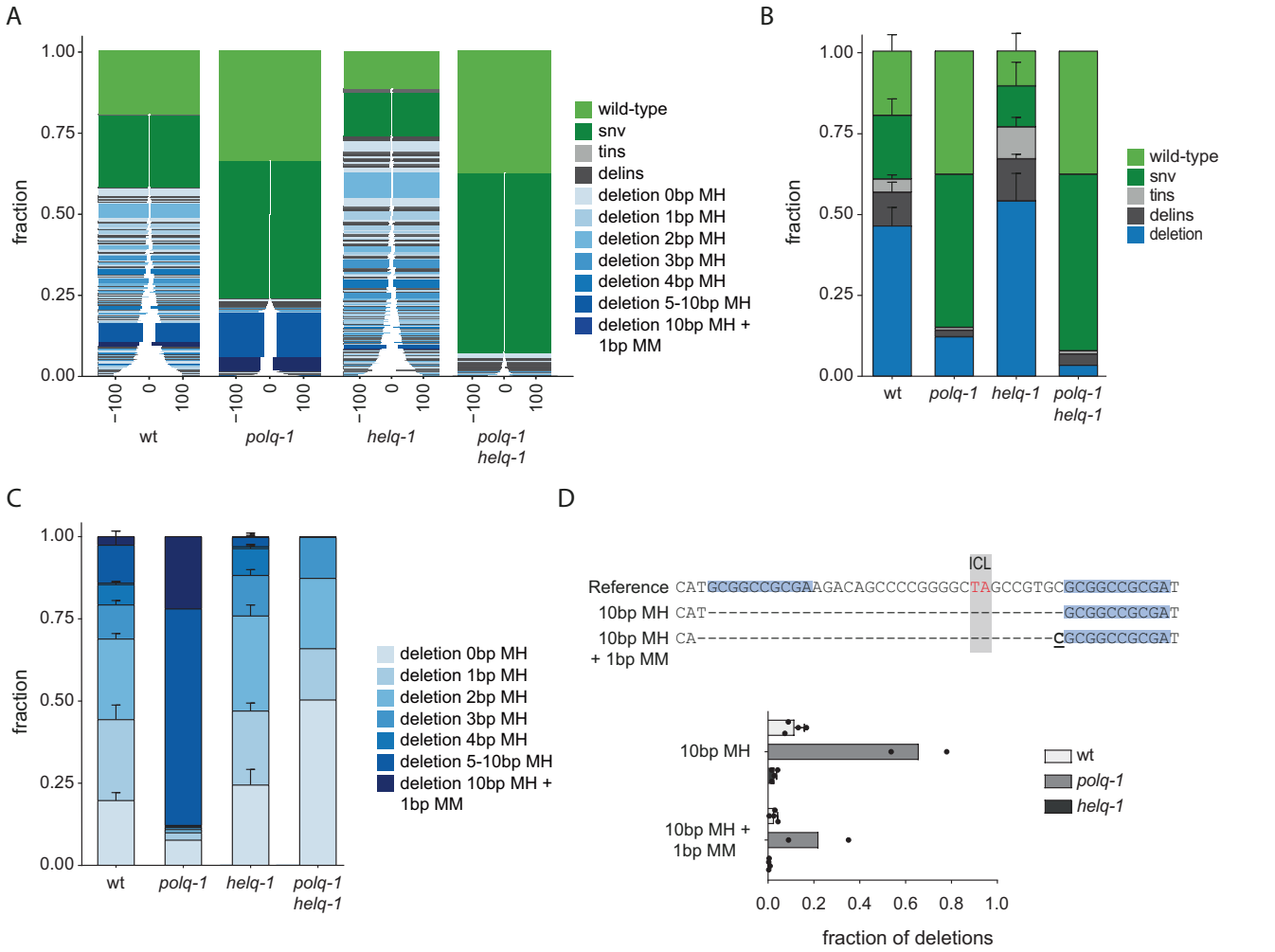

Fig. 3 | POLQ/HELQ-mediated INDEL mutagenesis at psoralen ICLs. A Tornado plots and **B** bar graphs representing the mutational spectrum for wild-type ($n = 5$), *polq-1* ($n = 2$), *helq-1* ($n = 3$) and *polq-1 helq-1* ($n = 2$) animals. Data are presented as mean values ± SD (for $n > 2$). **C** Bar graph depicting the length of microhomology observed at the deletion junctions, and their contribution to the deletion spectrum of the indicated genotype: wild-type ($n = 5$), *polq-1* ($n = 2$), *helq-1* ($n = 3$), and *polq-1 helq-1* ($n = 2$) animals. Data are presented as mean values ± SD (for $n > 2$). **D** Graphical representation of HELQ-dependent deletions either having 10 bp of perfect sequence homology or having 10 bp of sequence homology plus one non-matching nucleotide. Microhomology is highlighted in blue; the 1 bp mismatch is in bold and underlined. Bar graph shows the fraction of each outcome relative to the total deletion frequency for the indicated genotypes: wild-type ($n = 5$), *polq-1* ($n = 2$), *helq-1* ($n = 3$) animals. Data are presented as mean values ± SD (for $n > 2$). Source data are provided as a Source Data file.

surprisingly found that the FANCD2 (FCD-2) and FANCI (FNCI-1) status had no significant effect on the repair profile (Fig. 4A, B), also not when we adapted our assay to capture larger deletions by choosing primer sites further away from the ICL (350 bp at either site). These outcomes argue that the molecules onto which TLS and TMEJ act do not require FANCD2/FANCI functionality. Since ICL traverse is promoted by FANCD2[16], these results also imply that the ICL traverse pathway does not play a role in mutation induction in this system. In addition to the apparent absence of FANCD2/I contribution, also a deficiency of the structure-specific nuclease XPF (FANCQ)[43] did not alter the repair spectrum (Fig. 4A, B). Finally, we excluded a role for nucleotide excision repair and BRCA1-mediated homologous recombination in producing the ICL repair outcomes we monitor, as a deficiency of the core-NER factor XPA (Fig. 4) or of BRCA1 (Supplemental Figs. 2 and 4) did not change the overall profile.

TRAIP action ensures deletion junctions in close proximity to the ICL

These data raise the question whether the ICL repair we here monitor is in fact dependent on DNA replication, as previous work implicated converging replication forks as a prerequisite for the Fanconi anemia pathway to trigger ICL repair. Because a potential dependence on DNA replication cannot be addressed directly using a genetic whole animal model, we turned to investigate a replication fork modulating enzyme, i.e., TRAIP. This E3 ubiquitination ligase was recently demonstrated to facilitate ICL repair by ubiquitinating the DNA replicative helicase CMG complex (CDC45-MCM2-7-GINS) stalled at sites of ICLs upon dual fork convergence, leading to its unloading[4]. Subsequent to CMG unloading, the leading strand polymerase (paused at ~20–40 bp upstream of the ICL) can now progress toward the blocking lesion, which triggers the FA cascade[4]. To test whether TRAIP acts to facilitate repair of psoralen ICLs in *C. elegans* we generated a null allele of *trul-1*, the *C. elegans* TRAIP[44]. Animal development and fertility is not compromised by TRAIP loss (Supplemental Fig. 3 and ref. 44). We next established the ICL repair profile for *trul-1* mutant animals (Fig. 4C) and observed a striking consequence of TRAIP absence: the junctions of the deletions are further away from the ICL location; deletions are thus larger (Fig. 4C) as compared to those in TRAIP proficient animals. Figure 4D, in which we plotted the deletion junctions with respect to the ICL position, shows a dramatic underrepresentation of deletion junctions within ~15 nt of the ICL on both sides for *trul-1* mutant animals. The observation that the absence of TRAIP does not reduce TMEJ

https://doi.org/10.1038/s41467-025-57764-z

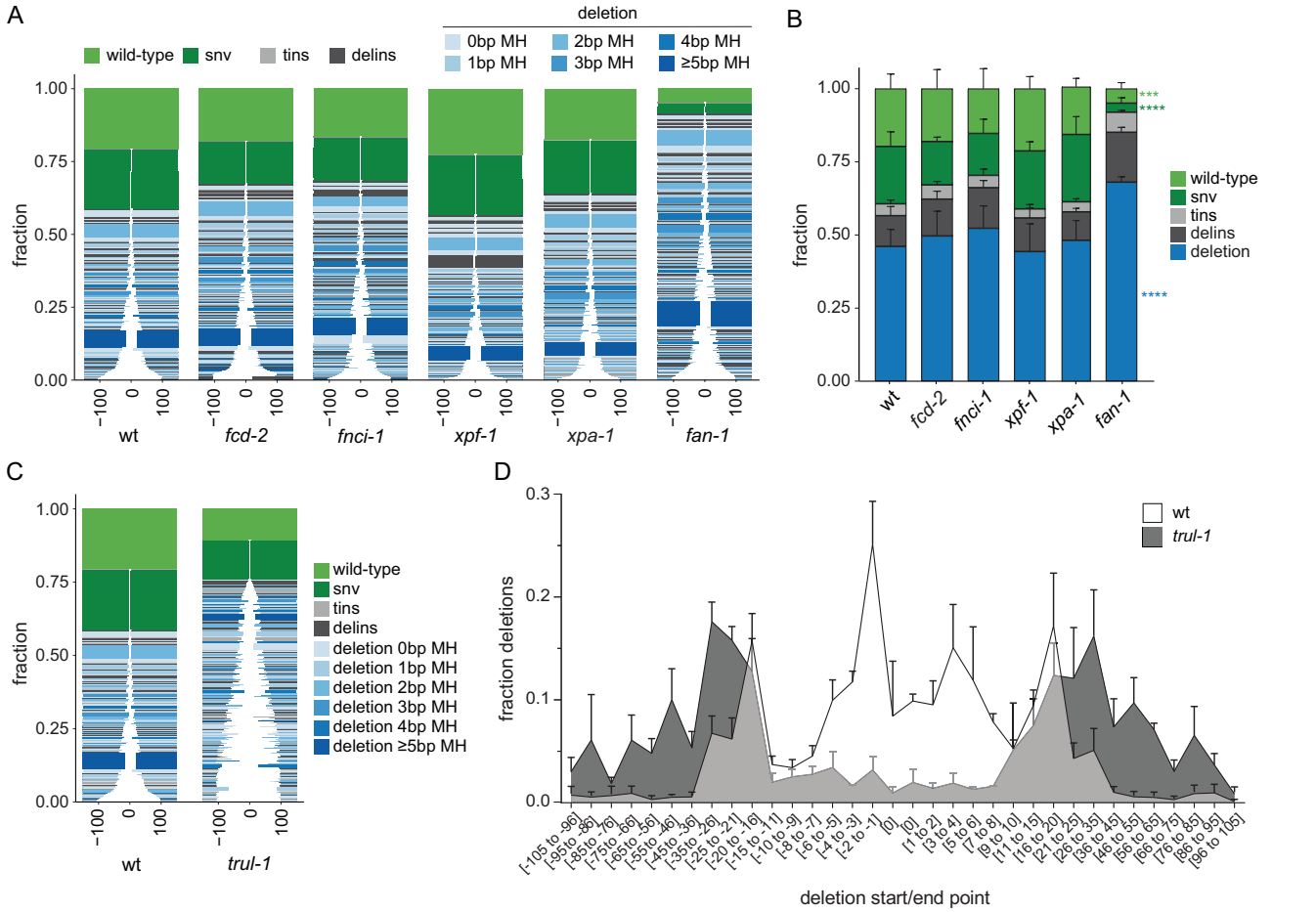

Fig. 4 | TRAIP and FAN1 deficiency differently affect psoralen ICL-induced mutagenesis. A Tornado plots and **B** bar graphs representing the mutational spectrum for wild-type ($n = 5$), *fcd-2* ($n = 3$), *fnci-1* (n = 3), *xpf-1* ($n = 3$), *xpa-1* ($n = 3$) and *fan-1* ($n = 3$) mutant animals (***$P = 0.0001$, ****$P < 0.0001$; Two-Way ANOVA test, Dunnett's multiple comparison test). Data are presented as mean values ± SD. **C** Tornado plots for wild-type ($n = 5$) and *trul-1* ($n = 3$) mutant animals. **D** Area plot of the position of the deletion junctions relative to the ICL location (x-axis) for wild-type ($n = 5$) and *trul-1* ($n = 3$) mutant animals. Y-axis represents the fraction of deletions within the deletion spectrum. Data are presented as mean values ± SD. Source data are provided as a Source Data file.

outcomes, but instead changes their configuration has important implications: First, the location of the deletion junctions further away from the ICL in *trul-1* mutant animals fits the hypothesis that TRAIP is required to remove the CMG helicase to allow the leading strand DNA polymerase to extend the nascent strand up to the ICL. This result is in line with the idea that the mode of ICL repair we are observing results from blocked DNA replication. Second, as the location of the deletion junction fits the proposed position of a blocked nascent strand, it argues that it is the 3′ hydroxyl end of the nascent leading strand that is a substrate for TMEJ action, and not necessarily a cleaved strand generated in the process of ICL unhooking. This may also explain why these products are not affected by loss of the FA pathway genes.

FAN1 promotes TLS of psoralen ICLs

While the *trul-1* data provide insight into the substrate molecules that feed into the TMEJ pathway, it does not provide insight into the molecules that are produced at the ICL site and are substrates for TLS: TLS necessitates incisions on one strand on either side of the crosslink. We found this unhooking step not promoted by the FA pathway involving XPF (Fig. 4A). In addition, *C. elegans* lacks many DNA glycosylases that are found in other species[45], including NEIL3, which disfavors unhooking by the previously described glycosylase pathway[15]; we also found that loss of the bifunctional endonuclease NTH-1 did not affect the repair profile (Supplemental Fig. 2). This argues for another biochemical activity that can convert an ICL into a TLS substrate. In an effort to unravel the mechanism underlying these TLS outcomes, we turned our attention to the *C. elegans* ortholog of the Fanconi Associated Nuclease 1 (FAN1). FAN1 deficiency leads to hypersensitivity to a wide range of ICL-inducing agents but does not cause Fanconi anemia[8–11,46]. Furthermore, cell sensitivity assays argue for a non-epistatic relationship: human cells deficient for both FAN1 and FANCC are more sensitive to the crosslinking agent cisplatin than either of the single mutants[47]. Together, these data suggest that FAN1 acts in a parallel pathway to the Fanconi anemia pathway, a notion supported by biochemical studies with purified FAN1, which demonstrated that this protein can act as a structure-specific nuclease with a preference for 5′ flap substrates, resembling a replication fork stalled at the ICL site[14,48]. We determined the outcome of psoralen ICL repair in worms lacking FAN1 and found *fan-1* mutant animals to produce a clearly aberrant profile: wild-type and SNV outcomes are largely absent (Fig. 4A, B), closely resembling the spectra in *polh-1*, *rev-1* and *rev-3* mutant animals (Fig. 2). The number of transgenic animals obtained by injecting *fan*-1 animals with psoralen-containing plasmids did not differ significantly from the number obtained from injecting wild-type animals (or other mutant backgrounds). Similarly, the number of distinct TMEJ outcomes within each repair profile remained constant. These two observations argue against the possibility that the absence of TLS products results from an indirect role of FAN1, such as in array formation. To further rule out this explanation, we conducted experiments where we co-injected an undamaged plasmid containing

https://doi.org/10.1038/s41467-025-57764-z

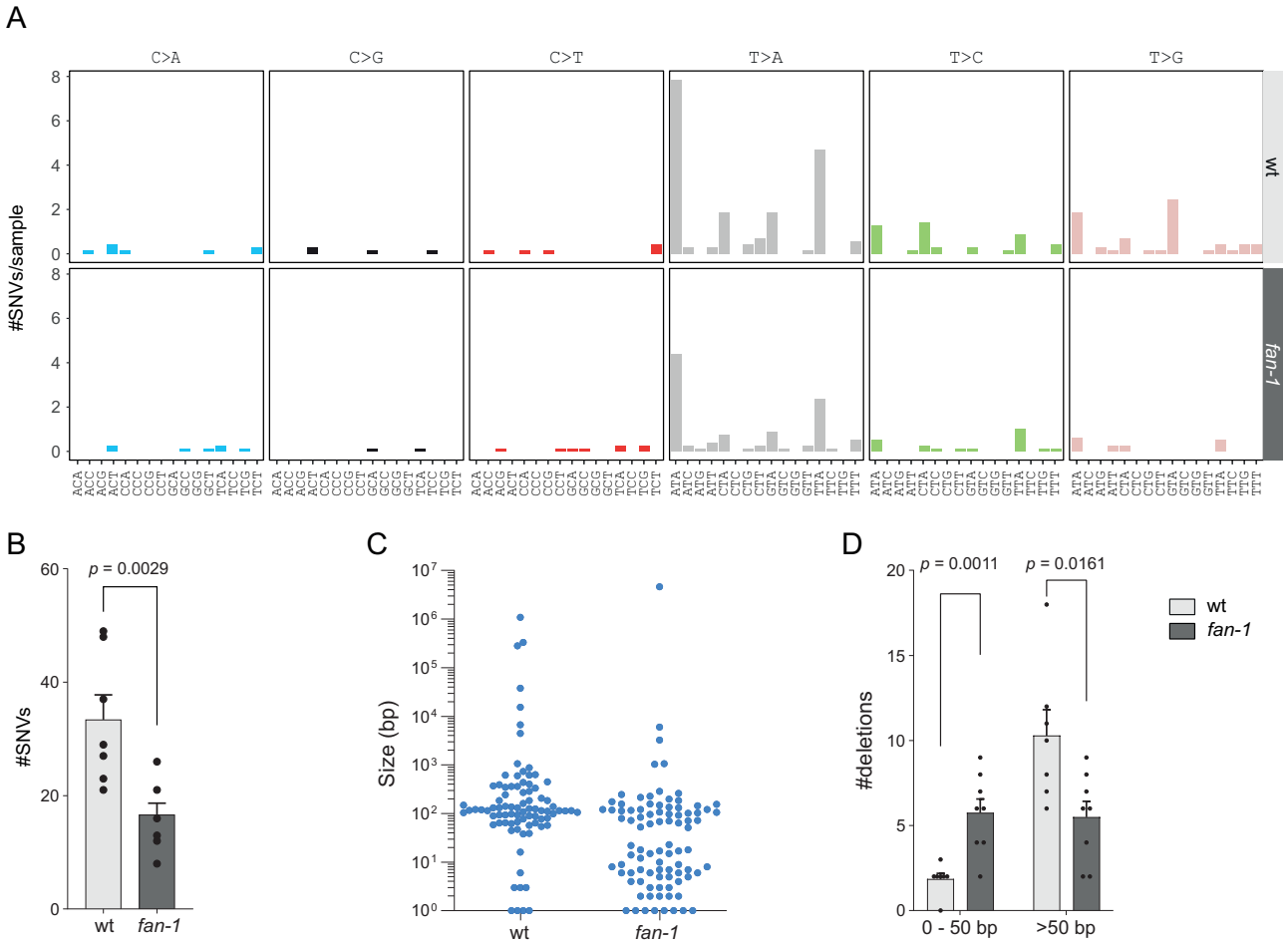

Fig. 5 | Genome alterations induced by psoralen treatment. A SNV pattern of UV-TMP treatment in wild-type ($n = 7$) and *fan-1* ($n = 8$) mutant animals, separated by nucleotidetype, and including the nucleotides that are immediately 5′ and 3′ to the mutation. **B** Bar graph comparing amount of SNVs between wild-type ($n = 7$) and *fan-1* ($n = 8$) mutant animals. Unpaired *T*-test was performed to assess significance ($p = 0.0029$; unpaired *t*-test, two-sided). Data are presented as mean values ± SEM. **C** Scatter plot showing deletions and their size (y-axis) for wild-type ($n = 7$) and *fan-1* samples ($n = 8$). **D** Bar graphs representing deletion size classes for wild-type ($n = 7$) and *fan-1* ($n = 8$) mutant animals (0–50 bp: $p = 0.0011$, >50 bp: $p = 0.0161$; unpaired *t*-test, two-sided). Data are presented as mean values ± SEM. Source data are provided as a Source Data file.

the same NGS primer binding sites as pICLpso. We hypothesized that a distorted ratio of both plasmids (as measured by NGS) could indicate a defect in incorporating damaged or repaired copies of pICLpso into the array. However, FAN1 deficiency did not alter this ratio (Supplemental Fig. 4). We thus propose that FAN1 directly contributes to ICL repair by generating TLS substrates.

TLS substates are rerouted to TMEJ in absence of FAN1

From the ICL repair profiles we cannot conclude whether the absence of wild-type and SNV outcomes may go together with a (similar) increase in TMEJ products: we are unable to discriminate uncompensated loss of a specific outcome from a scenario where the substrate molecules are rerouted toward another repair pathway. To address this question further and to investigate the fate of ICLs in the absence of FAN1 we used another method to detect repair products. We exposed animals to UV-TMP, which induces ICLs as well as monoadducts in the genomes of gametes, and subsequently sequenced the genomes of progeny animals. From UV-TMP exposed cultures of developmentally staged animals we isolated progeny that were resistant to nicotine and had a twitching phenotype, indicative of a loss-of-function mutation in the gene *unc-22*[49]. This way we are ensuring that the mutagenic treatment was effective; the *unc-22* mutation frequency in non-exposed populations is negligible as compared to exposed populations. Cultures were grown from single *unc-22* mutant animals after which DNA was isolated for whole-genome sequencing (WGS). It should be noted that accurate TLS of lesions will not be detected as that outcome cannot be distinguished from undamaged DNA; hence only products of mutagenic repair or mutagenic TLS will be detected. Figure 5A demonstrates that UV-TMP treatment induced an elevated frequency of SNVs specifically at nucleotides that are part of a TA configuration, which fits the expectation that the treatment causes psoralen linkages between thymines in opposite strands. Similar to the plasmid injection data, we found these SNVs to be the product of FAN1-mediated repair as the frequency is markedly reduced in *fan-1* mutant animals exposed to the same dose of UV-TMP (Fig. 5A, B). Conversely, we detected an increase in small deletions of 1–50 bp in *fan-1* mutant animals (Fig. 5C), which suggest that replication-blocking psoralen lesions in the absence of FAN1 are converted to DSBs that are repaired by TMEJ. In both wild-type and FAN1 deficient animals, we also find deletions of 50–300 bp in size (Fig. 5C, D), which we have previously investigated and are likely the result of psoralen monoadducts[19].

Discussion

Here, we have used plasmid injections into the germline of *C. elegans* to investigate ICL repair in vivo at nucleotide resolution. Previously, through whole-genome sequencing we and others have characterized

the types of mutations that were induced by exposing cells and animals to ICL-inducing agents[19,20,22]. However, that approach does not discriminate between ICLs, monoadducts or intra-strand crosslinks that can all be introduced by these agents. To overcome this complicating aspect, we developed a new in vivo method in which we monitor the spectrum of repair outcomes of a defined psoralen ICL. Through genetic analysis using mutant animals, we subsequently aimed to infer the mechanisms by which processing of these psoralen crosslinks confer genetic change. We established that psoralen ICLs induce two types of mutations: (i) SNVs, through POLH- and POLZ-mediated TLS, and (ii) deletions (plus or minus insertions) through POLQ- or HELQ-mediated end joining.

One of the key questions concerning the repair we monitored is whether the ICLs we introduce into the worm are repaired in a reaction that depends on DNA replication, as the current models, mostly based on detailed investigations using *Xenopus* egg extracts, argue for different biochemistry when an ICL is recognized as a replication fork barrier as opposed to a transcription-interfering lesion (or a lesion not impeding with these DNA metabolic processes)[1]. At present, we have only indirect support for proposing replication-dependent repair: the combined research in the field of *C. elegans* transgenesis supports a scenario where plasmids injected in the gonadal syncitium concatemerize in the cytoplasm of the fertilized zygote upon nuclear envelope breakdown of the first zygotic division[28] as if linearized plasmid molecules are then exposed to nucleus-contained DNA repair proteins that can use end joining and/or homology-directed repair pathways to ligate or stitch the plasmids together to form an extra-chromosomal array of, on average, 100–200 plasmid molecules[28]. It was shown through timelapse imaging that these extra-chromosomal arrays remain in an inert, yet chromatinized state, in the cytoplasm. Few of these arrays acquire segregation competency -the underlying biology is not yet understood- and then behave as chromosomes that can be stably segregated during cell division and over many animal generations, hence necessitating being replicated. It is also at this stage (in early embryonic cell divisions) that an extra-chromosomal array, by entering the nucleus, acquires transcription competence. We envision that it is after acquiring segregation competence that the psoralen ICLs within the original plasmid DNA are being recognized, as they pose a physical block to essential DNA metabolic processes. Psoralen ICLs may not be recognized independent of their blocking potential as we found that animals defective in nucleotide excision repair had mutation profiles similar to wild-type animals. Another rationale for implicating DNA replication in the ICL-induced mutagenesis we describe is that deletions brought about by TMEJ necessitate a double-strand break, and the only known routes in which a DSB is produced at an ICL involves replication forks generating a DSB upon incision of a parental strand. However, a stronger argument for inferring DNA replication is the observation that the junctions of resulting deletions are more distant from the position of the ICL in animals with compromised TRAIP action. This outcome is consistent with the reported role of TRAIP in replication-dependent ICL repair: removal of the obstructed CMG helicase preventing the processive DNA polymerases from synthesizing DNA all the way up to the ICL. Based on this result we envision that the 3′ end of the nascent strand acts as a substrate in a TMEJ reaction: In wild-type worms the ICL impedes DNA polymerase action, however, in TRAIP's absence it is the blocked and persistently present CMG helicase, halted by the ICL, that impedes DNA synthesis. As a consequence, TMEJ junctions are ~20 bp upstream of the ICL. The deletion junction may thus mark the site where the replicative polymerase arrests.

This interpretation of the data runs into a number of questions. For instance, what are the steps between ICL encounter and TMEJ? Two 3′ ends, generated by the nascent strands of a converging replication fork on either side of an ICL, can be processed by TMEJ but only if the substrate molecules are not still attached via the crosslink. In other words, what liberates the putative intermediates? The finding that mutations in FancD2 and FancI do not affect the repair profile disfavors FANC-dependent unhooking as a prerequisite for TMEJ. Indeed, apart from FANCD2/FANCI, also the FANC endonuclease XPF is not required for processing ICL substrates for TMEJ, nor is the nuclease that acts in a parallel pathway to the FANC proteins, i.e., FAN1. In fact, it appears that FAN1 acts to suppress TMEJ action: whole-genome sequencing of UV-TMP treated *fan-1* mutants displays more, not less TMEJ indels.

At present, we do not have an explanation for why the mutagenicity of psoralen ICLs does not require the FANC proteins. Whilst *C. elegans* does not encode the proteins that make up the FA core complex, there is sufficient data supporting a role for FancD2/I in counteracting crosslink damage also in this system[50,51]. We therefore do not consider a potential evolutionary distinction between worm and vertebrate ICL repair likely, but rather envision that we do not capture all forms of repair in our assay. We disfavor the explanation that repair of an ICL in a extra-chromosomal array may be different from that in the genome: the array is chromatinized and can be maintained for many animal generations arguing that it behaves as a normal chromosome, that is replicated leading to two sister copies that segregate into the two daughter cells upon cell division. One potential explanation that is consistent with other repair data previously generated for *C. elegans* is that early embryonic divisions do not allow for enough time to use "time-consuming" homologous recombination-mediated repair of DNA lesions. During early embryogenesis in nematodes, cells divide every 20 min and the cell cycle almost primarily consists of S and M phase[52]. It may thus be that in these embryonic stages, as suggested previously[31,53], the DNA damage response is set up to produce "quick-fixes": mutagenic joining of DSBs produced at replication-blocking lesions. Delay of the cell cycle by checkpoint activation has been shown to be detrimental to development, as replication-dependent checkpoints are in fact natural developmental triggers for asynchronous cell-division essential for patterning[54]. We thus entertain the idea that we have here provided insight into how fast-dividing cells, for which proper development may outweigh perfectly accurate copying of genetic information, deal with DNA lesions. This notion may be supported by the recent discovery of a mitotic pathway of replisome disassembly that can trigger replication fork collapse leading to POLQ-mediated DNA rearrangements[55]. It would be interesting to investigate whether the FA pathway is repressed in early embryogenic divisions, as has been suggested for other specific repair activities[53].

Concerning the non-deletion events, i.e., wild-type restoring and mutagenic bypass, we found POLH-1 and POLZ-1 to be the TLS polymerases required to bypass psoralen ICLs. We here identified the FAN1 endonuclease to also be required for TLS. FAN1 activity may produce the substrates onto which TLS polymerases can act, in agreement with earlier models for how FAN1 may process ICLs: incising one of the two strands and subsequently acting as an exonuclease removing the nucleotides surrounding the crosslinked bases[11,14,56,57]. The notion that TRAIP is grosso modo not required for TLS-mediated mutagenesis argues that this repair is independent of DNA replication. We therefore consider the option of two non-overlapping pathways to produce mutations at psoralen ICLs: replication-dependent TMEJ products of processed stalled-forks, and replication-independent TLS products, in which unhooking is induced by FAN1. In this respect it is of interest that individuals with germline mutations in FAN1 suffer from progressive kidney failure, an organ which, because of its function in filtering blood and transporting waste chemicals, is exposed to high levels of toxic agents. The inability of FAN1 mutated (possibly non-dividing) kidney cells to repair highly cytotoxic ICLs induced by environmental genotoxins or metabolic waste products may thus underlie the renal failure that develops in these KIN patients. Of additional interest, germline mutations in FAN1 have also been linked to cause hereditary colon cancer[58,59]. It would be of interest to determine whether these tumors have an elevated burden of small indels similar to the genomes of *C.*

elegans FAN1 deficient worms, in which the inability to perform FAN1-mediated TLS leads to the accumulation of small deletions.

Methods

Worm genetics

Nematodes were cultured on standard NGM plates seeded with OP50 bacteria at 20 °C[60]. The N2 Bristol strain was used as WT control. The following alleles were used in this study: *polq-1(tm2026), helq-1(tm2134), rev-3(gk919715), fcd-2(tm1298)*, *fnci-1(tm3081) fan-1(tm432), xpa-1(ok698), xpf-1(e1487), brc-1(lf249), trul-1(lf321), nth-1(ok724), rev-1(lf206)*. Some strains were provided by the CGC, which is funded by NIH Office of Research Infrastructure Programs (P40 OD010440). The *polh-1(lf31)*, *polk-1(lf29)*, *rev-1(lf206)* alleles were previously described[32].

CRISPR/Cas9-mediated generation of *trul-1* null allele

For CRISPR/Cas9-mediated targeting we used the following sequence (which includes the PAM site) in exon 1 of *trul-1*: GGTACCGAA-GAATGGATTTGTGG. Cloning was done as described in ref. 61. Plasmids were injected using standard *C. elegans* microinjection procedures. In brief, 1 day before injection, L4 animals were transferred to new plates and cultured at 15 degrees. Gonads of young adults were injected with a mix containing 20 ng/µl pDD162 (Peft-3::Cas9, Addgene 47549), 20 ng/µl pJJR50 (u6::sgRNA with *trul-1* target), 10 ng/µl pGH8, 2.5 ng/µl pCFJ90 and 5 ng/µl pCFJ104. Progeny (F1) animals that express mCherry were picked to new plates 3–4 days post-injection and allowed to produce offspring. Of each F1 plate 10 F2 animals were pooled, lysed and genotyped. Genotyping was done by PCR amplification of a 365 bp product around the CRISPR/Cas9 target site. A mutant was isolated with a 5 bp out-of-frame deletion (Supplemental Fig. 3).

NGS analysis of transgenic animals

Transgenic animals were created as follows: 20–24 h prior to injection, L4 animals were picked to fresh OP50 seeded NGM plates and incubated at 15 °C. Young adults were injected with an injection mix containing 100 ng/µl pRF4 (*rol-6(su1006)*) and 15 ng/µl pICLpso[62]. The ICL-containing plasmid pICLpso is described in ref. 63. Some genotypes were additionally injected with 5 ng/µl of an undamaged control plasmid pICLcon that differs from the pICLpso plasmid in the following manner at the ICL site: del: CGGGGC**TA**GC, ins: TCTTCCGC TCTTCTTT (location of ICL in pICLpso in bold). Injected P0 animals were subsequently singled to 6 cm dishes and 3 days post-injection these plates were checked for F1 rollers. Rollers were subsequently picked and pooled per 10 worms in 15 µl lysis buffer (50 mM KCl, 10 mM Tris-HCl pH 8.3, 2.5 mM $MgCl_2.6H_2O$, 0.45% NP40, 0.45% Tween-20) with ProtK (Merck #1.24568.0500, final concentration 0.5 mg/ml) and heated to 60 °C for 1 h and 95 °C for 15 min. 3 µl of each lysis with the same genotype was pooled to create a final lysis pool used to perform targeted sequencing PCR.

Primers (5′-GCCAGATTTTTCCTCCTCTCC-3′ and 5′-CAT-AGTCCCGCCCCTAACT-3′) specific for the ICL region were designed that yield a 254 bp product on wild-type alleles and that contain adapters for the p5 and p7 index primers (5′-: GATGTGTATAAGAGA-CAG -3′ and 5′- CGTGTGCTCTTCCGATCT -3′, respectively). These primers were used to amplify the targeted region using GoTaq G2 DNA polymerase (Promega) with the following conditions: 95 °C for 10 min, 25 cycles of 95 °C for 10 s, 54 °C for 30 s, and 72 °C for 30 s, and the final extension 72 °C for 5 min. The PCR products were purified using a 1.8× reaction volume of magnetic AMPure XP beads (Beckman Coulter) according to the manufacturer's protocol and DNA was eluted in 20 µl MQ. Flow-cell adapter sequences were added by performing PCRs with 5 µl purified PCR-product, 0.3 µM of p5 and p7 index primers and Phusion High-Fidelity DNA polymerase (Thermo Fisher Scientific) in a 20 µl reaction mix and the following conditions: 95 °C for 10 min, 5 cycles of 95 °C for 10 s, 58 °C for 30 s and 72 °C for 30 s, and the final extension 72 °C for 5 min. The PCR products were purified with 0.8× AMPure XP beads and eluted in 20 µl MQ. DNA concentrations were measured using the Quant-iT dsDNA assay kit and the Qubit Fluorometer (both Thermo Fisher Scientific) according to the manufacturer's protocol and samples were pooled at equimolar concentrations per PCR. Both quality and quantity of these pools were analyzed using a High Sensitivity DNA chip on an Agilent Bioanalyzer. The pools were sequenced on a NovaSeq6000 (Illumina) by 150-bp paired-end sequencing. In all separately carried out experiments in which mutant worms were assayed, also wild-type worms were included (in the entire procedure) to serve as controls for experimental variations.

Target sequencing bioinformatic analysis

Data was processed using SIQ software and the tornado graphs were made using the SIQPlotteR web-based tool[30].

Statistical analysis

GraphPad Prism software (9.3.1) was used for statistical analysis and production of the bar graphs and mountain plot. For mutational spectra and distribution of homology, two-way ANOVA statistical test was used. Statistical analysis for the UV-TMP data consisted of an unpaired *t*-test for the comparison of amount of SNVs and for the deletion size comparisons.

Twitcher assay

Worms are synchronized by incubating the worms in a 3:2 mixture of hypochlorite (Acros Organics) to 4 M NaOH until they were dissolved and only eggs remained. The eggs were washed with M9 buffer (22 mM KH_2PO_4, 42 mM Na_2HPO_4, 86 mM NaCl, 1 mM $MgSO_4$) to remove the residual bleach. Eggs were allowed to hatch overnight in M9 buffer. After hatching, larvae are plated on seeded 9 cm plates and allowed to grow to L4 stage. Animals were treated for one hour with 10 µg/ml TMP (Sigma, T6137, stock: 100 mg dissolved in 40 ml acetone) dissolved in M9, distributed onto non-seeded NGM plates and exposed to UVA irradiation (366 nm; CAMAG 29200 Universal UV LAMP) at a dose rate of 150 µW/cm^2, after which 10 animals were transferred to seeded 9 cm NGM plates. Population was allowed to grow until the F2 generation. Worms are washed and transferred into a 6-well plate. Levamisole (final concentration per well: 2 mM) is added and animals with a twitcher phenotype are picked and allowed to grow to a full population. If population non-twitchers are found in the population, twitchers are picked and again allowed to grow to a full homozygous twitcher population. After which genomic DNA was isolated using a Blood and Tissue Culture Kit (Qiagen). DNA was sequenced on an Illumina NovaSeq6000 platform.

Whole-genome sequencing bioinformatic analysis

Image analysis, base calling and error calibration were performed using standard Illumina software. BCL output from the Novaseq6000 platform was converted using the bcl2fastq tool. Raw reads were mapped to the *C. elegans* reference genome (Wormbase release 235) by BWA-mem[64] and SAMtools[65]. Pindel[66], Manta[67], Delly[68], Smoove[69] and GRIDSS[70] were used for calling structural variations. Variations were considered true if they were uniquely present in one of the samples and supported by at least two CNV callers and covered by at least 4 reads spanning the variant junction. In addition, CNV calls solely called by Pindel were added if at least 4 reads supporting the variant in a single sample were present and all other samples showed at least 8 reference-supporting reads and 0 variant-supporting reads. For SNV calling GATK HaplotypeCaller[71] was used. SNVs were only included if they occurred at a distance of at least 50 bp from any CNV junction and were uniquely found in a single sample.

Reporting summary

Further information on research design is available in the Nature Portfolio Reporting Summary linked to this article.

Data availability

The raw targeted sequence data generated in this study have been deposited at NCBI SRA under accession code: PRJNA1072310. Whole-genome sequence data generated in this study has been deposited at NCBI SRA under accession code: PRJNA1228572. Source data are provided with this paper.

References

1. Semlow, D. R. & Walter, J. C. Mechanisms of vertebrate DNA interstrand cross-link repair. *Annu. Rev. Biochem.* **90**, 107–135 (2021).
2. Niraj, J., Färkkilä, A. & D'Andrea, A. D. The Fanconi anemia pathway in cancer. *Annu. Rev. Cancer Biol.* **3**, 457–478 (2019).
3. Zhang, J. & Walter, J. C. Mechanism and regulation of incisions during DNA interstrand cross-link repair. *DNA Repair* **19**, 135–142 (2014).
4. Wu, R. A. et al. TRAIP is a master regulator of DNA interstrand crosslink repair. *Nature* **567**, 267–272 (2019).
5. Klein Douwel, D. et al. XPF-ERCC1 acts in unhooking DNA interstrand crosslinks in cooperation with FANCD2 and FANCP/SLX4. *Mol. Cell* **54**, 460–471 (2014).
6. Bhagwat, N. et al. XPF-ERCC1 participates in the Fanconi anemia pathway of cross-link repair. *Mol. Cell Biol.* **29**, 6427–6437 (2009).
7. Roy, U. & Schärer, O. D. Involvement of translesion synthesis DNA polymerases in DNA interstrand crosslink repair. *DNA Repair* **44**, 33–41 (2016).
8. Thongthip, S. et al. Fan1 deficiency results in DNA interstrand cross-link repair defects, enhanced tissue karyomegaly, and organ dysfunction. *Genes Dev.* **30**, 645–659 (2016).
9. Zhou, W. et al. FAN1 mutations cause karyomegalic interstitial nephritis, linking chronic kidney failure to defective DNA damage repair. *Nat. Genet.* **44**, 910–915 (2012).
10. Lachaud, C. et al. Karyomegalic interstitial nephritis and DNA damage-induced polyploidy in Fan1 nuclease-defective knock-in mice. *Genes Dev.* **30**, 639–644 (2016).
11. Kratz, K. et al. Deficiency of FANCD2-associated nuclease KIAA1018/FAN1 sensitizes cells to interstrand crosslinking agents. *Cell* **142**, 77–88 (2010).
12. Liu, T., Ghosal, G., Yuan, J., Chen, J. & Huang, J. FAN1 acts with FANCI-FANCD2 to promote DNA interstrand cross-link repair. *Science* **329**, 693–696 (2010).
13. Pizzolato, J., Mukherjee, S., Schärer, O. D. & Jiricny, J. FANCD2-associated nuclease 1, but not exonuclease 1 or flap endonuclease 1, is able to unhook DNA interstrand cross-links in vitro. *J. Biol. Chem.* **290**, 22602–22611 (2015).
14. Wang, R. et al. Mechanism of DNA interstrand cross-link processing by repair nuclease FAN1. *Science* **346**, 1127–1130 (2014).
15. Semlow, D. R., Zhang, J., Budzowska, M., Drohat, A. C. & Walter, J. C. Replication-dependent unhooking of DNA interstrand cross-links by the NEIL3 glycosylase. *Cell* **167**, 498–511.e14 (2016).
16. Huang, J. et al. The DNA translocase FANCM/MHF promotes replication traverse of DNA interstrand crosslinks. *Mol. Cell* **52**, 434–446 (2013).
17. Huang, J. et al. Remodeling of interstrand crosslink proximal replisomes is dependent on ATR, FANCM, and FANCD2. *Cell Rep.* **27**, 1794–1808.e5 (2019).
18. Williams, H. L., Gottesman, M. E. & Gautier, J. Replication-independent repair of DNA interstrand crosslinks. *Mol. Cell* **47**, 140–147 (2012).
19. van Schendel, R., van Heteren, J., Welten, R. & Tijsterman, M. Genomic scars generated by polymerase theta reveal the versatile mechanism of alternative end-joining. *PLoS Genet.* **12**, e1006368 (2016).
20. Volkova, N. V et al. Mutational signatures are jointly shaped by DNA damage and repair. *Nat. Commun.* **11**, 2169 (2020).
21. Budzowska, M., Graham, T. G. W., Sobeck, A., Waga, S. & Walter, J. C. Regulation of the Rev1–pol ζ complex during bypass of a DNA interstrand cross-link. *EMBO J.* **34**, 1971–1985 (2015).
22. Kucab, J. E. et al. A compendium of mutational signatures of environmental agents. *Cell* **177**, 821–836.e16 (2019).
23. Tucker, M. A., Coleman, C. N., Cox, R. S., Varghese, A. & Rosenberg, S. A. Risk of second cancers after treatment for hodgkin's disease. *N. Engl. J. Med.* **318**, 76–81 (1988).
24. Travis, L. B. et al. Risk of leukemia after platinum-based chemotherapy FOR OVARian Cancer. *N. Engl. J. Med.* **340**, 351–357 (1999).
25. Räschle, M. et al. Mechanism of replication-coupled DNA interstrand crosslink repair. *Cell* **134**, 969–980 (2008).
26. Knipscheer, P. et al. The Fanconi anemia pathway promotes replication-dependent DNA interstrand cross-link repair. *Science* **326**, 1698–1701 (2009).
27. Zhang, J. et al. DNA interstrand cross-link repair requires replication-fork convergence. *Nat. Struct. Mol. Biol.* **22**, 242–247 (2015).
28. Yuen, K. W. Y., Nabeshima, K., Oegema, K. & Desai, A. Rapid de novo centromere formation occurs independently of heterochromatin protein 1 in C. elegans embryos. *Curr. Biol.* **21**, 1800–1807 (2011).
29. Mello, C. C., Kramer, J. M., Stinchcomb, D. & Ambros, V. Efficient gene transfer in C. elegans: extrachromosomal maintenance and integration of transforming sequences. *EMBO J.* **10**, 3959–3970 (1991).
30. van Schendel, R., Schimmel, J. & Tijsterman, M. SIQ: easy quantitative measurement of mutation profiles in sequencing data. *NAR Genom. Bioinform.* **4**, lqac063 (2022).
31. Roerink, S. F., Koole, W., Stapel, L. C., Romeijn, R. J. & Tijsterman, M. A broad requirement for TLS polymerases η and κ, and interacting sumoylation and nuclear pore proteins, in lesion bypass during C. elegans embryogenesis. *PLoS Genet.* **8**, e1002800 (2012).
32. van Bostelen, I., van Schendel, R., Romeijn, R. & Tijsterman, M. Translesion synthesis polymerases are dispensable for C. elegans reproduction but suppress genome scarring by polymerase theta-mediated end joining. *PLoS Genet.* **16**, e1008759 (2020).
33. Ohmori, H., Hanafusa, T., Ohashi, E. & Vaziri, C. Separate roles of structured and unstructured regions of Y-family DNA polymerases. *Adv. Protein Chem. Struct. Biol.* **78**, 99–146 (2009).
34. Prakash, S., Johnson, R. E. & Prakash, L. Eukaryotic translesion synthesis DNA polymerases: specificity of structure and function. *Annu. Rev. Biochem.* **74**, 317–353 (2005).
35. Niedzwiedz, W. et al. The Fanconi anaemia gene FANCC promotes homologous recombination and error-prone DNA repair. *Mol. Cell* **15**, 607–620 (2004).
36. Sale, J. E., Lehmann, A. R. & Woodgate, R. Y-family DNA polymerases and their role in tolerance of cellular DNA damage. *Nat. Rev. Mol. Cell Biol.* **13**, 141–152 (2012).
37. Bezalel-Buch, R., Cheun, Y. K., Roy, U., Schärer, O. D. & Burgers, P. M. Bypass of DNA interstrand crosslinks by a Rev1–DNA polymerase ζ complex. *Nucleic Acids Res.* **48**, 8461–8473 (2020).
38. Roerink, S. F., van Schendel, R. & Tijsterman, M. Polymerase theta-mediated end joining of replication-associated DNA breaks in C. elegans. *Genome Res.* **24**, 954–962 (2014).
39. Schimmel, J., van Schendel, R., den Dunnen, J. T. & Tijsterman, M. Templated insertions: a smoking gun for polymerase theta-mediated end joining. *Trends Genet.* **35**, 632–644 (2019).

40. Kamp, J. A. et al. Helicase Q promotes homology-driven DNA double-strand break repair and prevents tandem duplications. *Nat. Commun.* **12**, 7126 (2021).
41. Crossan, G. P. & Patel, K. J. The Fanconi anaemia pathway orchestrates incisions at sites of crosslinked DNA. *J. Pathol.* **226**, 326–337 (2011).
42. Collis, S. J., Barber, L. J., Ward, J. D., Martin, J. S. & Boulton, S. J. C. elegans FANCD2 responds to replication stress and functions in interstrand cross-link repair. *DNA Repair)* **5**, 1398–1406 (2006).
43. Saito, T. T., Youds, J. L., Boulton, S. J. & Colaiácovo, M. P. Caenorhabditis elegans HIM-18/SLX-4 interacts with SLX-1 and XPF-1 and maintains genomic integrity in the germline by processing recombination intermediates. *PLoS Genet.* **5**, e1000735 (2009).
44. Sonneville, R. et al. TRAIP drives replisome disassembly and mitotic DNA repair synthesis at sites of incomplete DNA replication. *eLife* **8**, e48686 (2019).
45. Elsakrmy, N., Zhang-Akiyama, Q.-M. & Ramotar, D. The base excision repair pathway in the nematode Caenorhabditis elegans. *Front. Cell Dev. Biol.* **8**, 598860 (2020).
46. Deshmukh, A. L. et al. FAN1, a DNA repair nuclease, as a modifier of repeat expansion disorders. *J. Huntingt. Dis.* **10**, 95–122 (2021).
47. Yoshikiyo, K. et al. KIAA1018/FAN1 nuclease protects cells against genomic instability induced by interstrand cross-linking agents. *Proc. Natl Acad. Sci. USA* **107**, 21553–21557 (2010).
48. MacKay, C. et al. Identification of KIAA1018/FAN1, a DNA Repair Nuclease Recruited to DNA Damage by Monoubiquitinated FANCD2. *Cell* **142**, 65–76 (2010).
49. Moerman, D. G. & Baillie, D. L. Genetic organization in caenorhabditis elegans: fine-structure analysis of the unc-22 gene. *Genetics* **91**, 95–103 (1979).
50. Youds, J. L., Barber, L. J. & Boulton, S. J. C. elegans: a model of Fanconi anemia and ICL repair. *Mutat. Res.* **668**, 103–116 (2009).
51. Wilson, D. M., Rieckher, M., Williams, A. B. & Schumacher, B. Systematic analysis of DNA crosslink repair pathways during development and aging in Caenorhabditis elegans. *Nucleic Acids Res.* **45**, 9467–9480 (2017).
52. Schierenberg, E. & Wood, W. B. Control of cell-cycle timing in early embryos of Caenorhabditis elegans. *Dev. Biol.* **107**, 337–354 (1985).
53. Holway, A. H., Kim, S.-H., La Volpe, A. & Michael, W. M. Checkpoint silencing during the DNA damage response in Caenorhabditis elegans embryos. *J. Cell Biol.* **172**, 999–1008 (2006).
54. Brauchle, M., Baumer, K. & Gönczy, P. Differential activation of the DNA replication checkpoint contributes to asynchrony of cell division in C. elegans embryos. *Curr. Biol.* **13**, 819–827 (2003).
55. Deng, L. et al. Mitotic CDK promotes replisome disassembly, Fork Breakage, and complex DNA rearrangements. *Mol. Cell* **73**, 915–929.e6 (2019).
56. Zhao, Q., Xue, X., Longerich, S., Sung, P. & Xiong, Y. Structural insights into 5′ flap DNA unwinding and incision by the human FAN1 dimer. *Nat. Commun.* **5**, 5726 (2014).
57. Gwon, G. H. et al. Crystal structure of a Fanconi anemia-associated nuclease homolog bound to 5′ flap DNA: basis of interstrand cross-link repair by FAN1. *Genes Dev.* **28**, 2276–2290 (2014).
58. Seguí, N. et al. Germline mutations in FAN1 cause hereditary colorectal cancer by impairing DNA repair. *Gastroenterology* **149**, 563–566 (2015).
59. Smith, A. L. et al. Candidate DNA repair susceptibility genes identified by exome sequencing in high-risk pancreatic cancer. *Cancer Lett.* **370**, 302–312 (2016).
60. Brenner, S. The genetics of Caenorhabditis elegans. *Genetics* **77**, 71–94 (1974).
61. Waaijers, S. et al. CRISPR/Cas9-targeted mutagenesis in Caenorhabditis elegans. *Genetics* **195**, 1187–1191 (2013).
62. Kadandale, P., Chatterjee, I. & Singson, A. Germline transformation of Caenorhabditis elegans by injection. *Methods Mol. Biol.* **518**, 123–133 (2009).
63. Knipscheer, P., Räschle, M., Schärer, O. D. & Walter, J. C. Replication-coupled DNA interstrand cross-link repair in Xenopus egg extracts. *Methods Mol. Biol.* **920**, 221–243 (2012).
64. Li, H. & Durbin, R. Fast and accurate short read alignment with Burrows–Wheeler transform. *Bioinformatics* **25**, 1754–1760 (2009).
65. Danecek, P. et al. Twelve years of SAMtools and BCFtools. *Gigascience* **10**, giab008 (2021).
66. Ye, K., Schulz, M. H., Long, Q., Apweiler, R. & Ning, Z. Pindel: a pattern growth approach to detect break points of large deletions and medium sized insertions from paired-end short reads. *Bioinformatics* **25**, 2865–2871 (2009).
67. Chen, X. et al. Manta: rapid detection of structural variants and indels for germline and cancer sequencing applications. *Bioinformatics* **32**, 1220–1222 (2015).
68. Rausch, T. et al. DELLY: structural variant discovery by integrated paired-end and split-read analysis. *Bioinformatics* **28**, i333–i339 (2012).
69. Pedersen, B. S., Layer, R. & Quinlan, A. R. Smoove: structural variant calling and genotyping with existing tools (Version 0.2.8) [Computer software] (2020).
70. Cameron, D. L. et al. GRIDSS: sensitive and specific genomic rearrangement detection using positional de Bruijn graph assembly. *Genome Res.* **27**, 2050–2060 (2017).
71. Poplin, R. et al. Scaling accurate genetic variant discovery to tens of thousands of samples. Preprint at *bioRxiv* https://doi.org/10.1101/201178 (2017).

Acknowledgements

Some strains were provided by the CGC, which is funded by NIH Office of Research Infrastructure Programs (P40 OD010440). This work was funded by an ALW OPEN grant (OP.393) from The Netherlands Organization for Scientific Research for Earth and Life Sciences to M.T.

Author contributions

R.v.S. and M.T. conceived and designed the study. J.V., R.v.S., and I.v.B. performed the experiments. R.v.S. performed the bioinformatical analyses. A.V. generated ICL-containing plasmids. J.V., R.v.S., P.K., and M.T. interpreted the experimental results. J.V. and M.T. wrote the manuscript which was reviewed and edited by all other authors.

Competing interests

The authors declare no competing interests.

Additional information

Supplementary information The online version contains supplementary material available at https://doi.org/10.1038/s41467-025-57764-z.

Correspondence and requests for materials should be addressed to Marcel Tijsterman.

Peer review information *Nature Communications* thanks Orlando Scharer and the other, anonymous, reviewer(s) for their contribution to the peer review of this work. A peer review file is available.